

Charge Density Wave Ordering in NdNiO₂: Effects of Multiorbital Nonlocal Correlations

Evgeny A. Stepanov,^{1,2} Matteo Vandelli,³ Alexander I. Lichtenstein,^{4,3} and Frank Lechermann⁵

¹CPHT, CNRS, École polytechnique, Institut Polytechnique de Paris, 91120 Palaiseau, France

²Collège de France, Université PSL, 11 place Marcelin Berthelot, 75005 Paris, France

³The Hamburg Centre for Ultrafast Imaging, Luruper Chaussee 149, 22761 Hamburg, Germany

⁴Institut für Theoretische Physik, Universität Hamburg, Notkestraße 9, 22607 Hamburg, Germany

⁵Institut für Theoretische Physik III, Ruhr-Universität Bochum, D-44780 Bochum, Germany

In this work, we investigate collective electronic fluctuations and, in particular, the possibility of the charge density wave ordering in an infinite-layer NdNiO₂. We perform advanced many-body calculations for the *ab-initio* three-orbital model by taking into account local correlation effects, nonlocal charge and magnetic fluctuations, and the electron-phonon coupling. We find that in the considered material, electronic correlations are strongly orbital- and momentum-dependent. Notably, the charge density wave and magnetic instabilities originate from distinct orbitals. In particular, we show that the correlation effects lead to the momentum-dependent hybridization between different orbitals, resulting in the splitting and shifting of the flat part of the Ni- d_{z^2} band. This strong renormalization of the electronic spectral function drives the charge density wave instability that is related to the intraband Ni- d_{z^2} correlations. Instead, the magnetic instability stems from the Ni- $d_{x^2-y^2}$ orbital, which remains half-filled through the redistribution of the electronic density between different bands even upon hole doping. Consequently, the strength of the magnetic fluctuations remains nearly unchanged for the considered doping levels. We argue that this renormalization is not inherent to the stoichiometric case but can be induced by hole doping.

INTRODUCTION

The discovery of superconductivity (SC) in layered nickel-oxide compounds, has been one of the most thrilling research findings in the recent years. It started off from revealing SC in thin-films of infinite-layer nickelates upon hole doping δ with $T_c \sim 15$ K [1–5], and afterwards also in low-valence multilayer nickelates [6]. As a last key development, high- T_c SC with $T_c \sim 80$ K has been uncovered in the pressurized bilayer compound La₃Ni₂O₇ [7]. Unconventional SC is often escorted by other electronic orders in an intriguing phase diagram, but the usual suspect of magnetic-ordering kind remains elusive in these nickelates. However, there have been several experimental reports of charge-density wave (CDW) ordering in the thin-films of rare-earth infinite-layer nickelates, originating at stoichiometry and stable up to ambient temperatures. This detected CDW order is associated with an in-plane incommensurate wave vector $\mathbf{q}_{\text{CDW}} \sim (0.3, 0)$ and involves Ni(3d) and rare-earth(5d) degrees of freedom [8–11]. But recently, a debate has started about the role of the substrate and of possible impurity phases in view of the CDW findings in these thin-film systems [12–16].

The theoretical modelling of the correlated electronic structure of superconducting nickelates is also not yet settled. The physics of these systems is governed by a complex interplay between strong local Coulomb correlations, spatial collective electronic fluctuations, orbital degrees of freedom, and a non-trivial band structure. Density functional theory (DFT) calculations for infinite-layer nickelates [17, 18] describe a nearly half-filled Ni- $d_{x^2-y^2}$ -dominated band at the Fermi level, with additional electron pockets from a self-doping (SD) band (solid black lines in Fig. 1). Around the Γ point, the latter is based on significant contribution from Ni- d_{z^2} and Nd- d_{z^2} . In addition, at $k_z = \pi$ momentum the Ni- d_{z^2} band displays a flat

part, which may trigger various collective electronic instabilities if appearing at the Fermi energy [19–21]. Until now, even the most advanced numerical calculations could not account for all these important effects simultaneously. Especially for these low-valence $3d^{9-\delta}$ systems of infinite-layer and multilayer kind, there is thus an ongoing debate concerning the picture most-effectively describing the low-energy physics: a single dominant Ni- $d_{x^2-y^2}$ orbital [22–32] versus a mainly Ni- e_g multi-orbital character [18, 33–38]. Neglecting spatial collective electronic fluctuations makes possible the *state-of-the-art* dynamical mean-field theory (DMFT) [39] calculations for an *ab-initio* multi-orbital model. On the other hand, a single-orbital description allows for accounting for the spatial correlation effects that are missing in DMFT [27, 40]. The correlation strength in different model calculations varies from a weakly-to-moderately metallicity up to (orbital-selective) Mott-critical regimes. In view of a possible CDW ordering, calculations which in the end focus on a dominant Ni- $d_{x^2-y^2}$ low-energy degree of freedom may indeed give reason for the experimentally detected incommensurate order [41, 42].

In this work, the possibility of a CDW instability in the infinite-layer nickelate NdNiO₂, at stoichiometry as well as upon hole doping, is examined by a model Hamiltonian study based on its realistic low-energy electronic structure. This modeling goes beyond the sole Ni- $d_{x^2-y^2}$ -based physics, allowing for multi-orbital Ni- e_g processes interplaying with the SD band. Furthermore, our numerical approach accounts for the combined effect of strong local electronic correlations, nonlocal collective electronic fluctuations, and phonon degrees of freedom. This surpasses any theoretical description ever performed for this class of materials.

Our results demonstrate that accounting for both spatial electronic correlations and orbital degrees of freedom is important. We find that the nonlocal electronic correlations in NdNiO₂ result in a substantial momentum- and orbital-

dependent renormalization and hybridization of all bands considered in our *ab-initio* model, which cannot be captured neither on the basis of local theories nor within a single-band framework. As a main result, we show that the CDW ordering in the infinite-layer NdNiO₂ originates from the intraband correlations within the Ni- d_{z^2} orbital. Upon the renormalization, the flat part of this band, which originally lies below the Fermi level, splits into two parts. One part moves toward the Fermi energy and can even appear above the Fermi level. The other part moves in the opposite direction and hybridizes with the lower Hubbard band of the Ni- $d_{x^2-y^2}$ orbital. In addition, we find that electronic correlations enlarge the electron pocket around the Γ point, which corresponds to the hybridized Ni- d_{z^2} and SD bands. This enhancement eventually leads to the nesting of the Fermi surface and to the CDW instability.

We argue that such momentum-dependent renormalization of the electronic spectral function is unlikely to occur at stoichiometry, in agreement with recent experimental works that conclude on the absence of the CDW instability in the undoped case [12, 13, 16]. However, we further demonstrate that the CDW instability can be induced upon hole doping the system. Remarkably, the estimated critical value of the electronic density for the CDW phase transition agrees well with the position of the dip in the superconducting dome observed in the hole doped NdNiO₂ [1, 2]. This fact suggests that the SC state in this material might be in a strong interplay with the CDW fluctuations. A similar conclusion was also reported in a recent experimental work [43], where the rotational symmetry breaking observed in superconducting Nd_{0.8}Sr_{0.2}NiO₂ films was associated with the charge ordering.

RESULTS

Model. In order to describe explicit many-body effects in NdNiO₂ we use a minimal 3-orbital $\{d_{z^2}, d_{x^2-y^2}, \text{SD}\}$ model that accounts for an almost occupied Ni- d_{z^2} orbital, a half-filled Ni- $d_{x^2-y^2}$ orbital, and a nearly empty self-doping (SD) band. To this end, the 3-orbital Wannier Hamiltonian derived in Ref. [34] from DFT calculations for NdNiO₂ is taken and supplemented with local interactions. The resulting three-orbital Hubbard-Holstein-Kanamori Hamiltonian reads:

$$H = \sum_{jj',\sigma,l} t_{jj'}^{ll'} c_{j\sigma l}^\dagger c_{j'\sigma l'} + \frac{1}{2} \sum_{j,\{l_i\},\{\sigma\}} U_{l_1 l_2 l_3 l_4} c_{j\sigma l_1}^* c_{j\sigma l_2}^* c_{j\sigma l_3} c_{j\sigma l_4} + \omega_{\text{ph}} \sum_j b_j^\dagger b_j + \lambda \sum_j n_j (b_j + b_j^\dagger), \quad (1)$$

where $c_{j\sigma l}^{(\dagger)}$ operator describes annihilation (creation) of an electron on the site j on the band l with the spin projection $\sigma = \{\uparrow, \downarrow\}$. The dispersion of the electrons is defined by the hopping amplitudes $t_{jj'}^{ll'}$ that are obtained from *ab-initio* calculations. The on-site interaction $U_{l_1 l_2 l_3 l_4}$ for $l_i \in \{d_{z^2}, d_{x^2-y^2}\}$ bands is taken in the Kanamori form that includes the intra-orbital $U_{lll} = U$, interorbital $U_{ll'l'} = U' = U - 2J$, spin flip

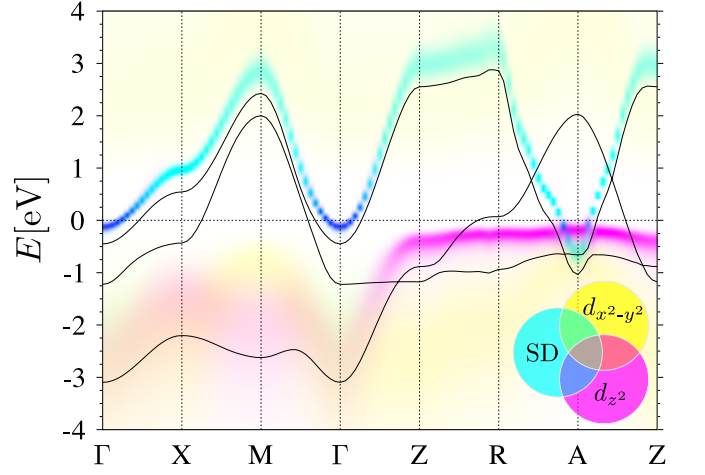


FIG. 1. The momentum-resolved electronic spectral function. The result is obtained at half filling for μ_{xy} using LDA (solid black lines) and DMFT (see the inset for the color code) for the d_{z^2} , $d_{x^2-y^2}$, and SD bands along the high-symmetry path in the BZ.

$U_{ll'l} = J$, and pair hopping $U_{ll'l'} = J$ terms. The intra-orbital term is set to $U = 7$ eV and the Hund's rule coupling to $J = 1$ eV [34]. The SD band is considered uncorrelated, so $U_{l_1 l_2 l_3 l_4} = 0$ if any index l_i belongs to SD.

The second line in Eq. (1) describes the effect of phonons. The operator $b_j^{(\dagger)}$ annihilates (creates) a phonon on the site j . The phonon operators are coupled to the electronic density operator defined as $n_j = \sum_{j,\sigma,l} c_{j\sigma l}^\dagger c_{j\sigma l}$. The phonon frequency $\omega_{\text{ph}} = 24.4$ meV (283 K) and the electron-phonon coupling $\lambda = 0.22$ are approximated with a local phonon model following Ref. [17]. For convenience, we integrate out phonon operators, which results in an effective local frequency-dependent attractive interaction $U_{ll'l'}^{\text{ph}}(\omega) = -2\lambda^2 \frac{\omega_{\text{ph}}}{\omega_{\text{ph}}^2 - \omega^2}$ between the electronic densities [44–47].

Strong electronic correlations in NdNiO₂ manifest themselves in the formation of Hubbard bands and in the orbital-selective Mott behavior of the material [34]. Taking these effects into account requires using DMFT that accurately describes local electronic correlations. Addressing many-body instabilities related to spatial collective electronic fluctuations, e.g. the formation of the CDW ordering, requires using diagrammatic extensions of DMFT [48, 49] that can efficiently treat momentum-dependent electronic correlations. We use the dual triply irreducible local expansion (D-TRILEX) method [50–52], which consistently accounts for the effect of local correlations and spatial collective electronic fluctuations of an arbitrary range within a broad set of model parameters [47, 53–55]. In this method, local electronic correlations are taken into account exactly by solving the DMFT impurity problem using continuous time quantum Monte Carlo solvers [56–59]. In this work, the impurity problem is solved using the w2DYNAMICS package [60]. The spatial collective electronic fluctuations are treated approximately by considering the leading (particle-hole ladder-like)

diagrammatic contributions to the self-energy and the polarization operator [50–52]. In this way, the method provides a self-consistent many-body solution to the problem at the level of both, single- (electronic Green’s function) and two-particle (charge, spin, and orbital susceptibilities) response functions with full momentum and frequency dependence. The advantage of D-TRILEX is that it has a much simpler diagrammatic structure compared to other extensions of DMFT, enabling tractable numerical calculations in the multi-orbital framework [61–64]. In particular, the D-TRILEX method does not involve the four-point vertex function, the calculation [59, 60, 65] and utilization of which in the diagrammatic expansion [66–68] significantly complicates numerical calculations in the multi-orbital case. Despite a rather simple structure, D-TRILEX operates on the same level of accuracy as much more advanced diagrammatic approaches [51, 52, 69], which is achieved by considering important local three-point (Hedin [70]) vertex corrections in the self-energy and the polarization operator. The main drawback of the current method implementation is its restriction to the non-symmetry-broken phase. This limitation is shared with the majority of other diagrammatic extensions of DMFT, although there have been several attempts to perform diagrammatic calculations in the symmetry-broken phases (see, e.g., Refs. [71–75]). It means, that D-TRILEX can capture the formation of the ordered state by the divergence of the corresponding susceptibility (the momentum \mathbf{q} , at which the susceptibility diverges, corresponds to the wave vector of the ordering), but cannot perform calculations inside the ordered phases. This limitation sometimes restricts D-TRILEX calculations to a rather high-temperature regime if the system reveals magnetic instability already at high temperatures, as happens, e.g., in the considered case. Details on the many-body calculations are provided in the Methods section.

Formation of the CDW at half filling. The half-filled case of $n_{\text{total}} = 3$ electrons per three $\{d_{z^2}, d_{x^2-y^2}, \text{SD}\}$ bands corresponds to NdNiO₂ at stoichiometry. DFT in local-density approximation (LDA) (i.e. the formal $U = 0$ case) predicts an exotic band structure for the system with the following occupation of the bands: $\{n_{z^2}, n_{x^2-y^2}, n_{\text{SD}}\} = \{1.84, 0.93, 0.23\}$ [34]. The electronic band structure of LDA is shown in Fig. 1 in solid black lines. The result is calculated along the high-symmetry path in the Brillouin Zone (BZ) that consists of the $\Gamma = (0, 0, 0)$, X = $(\pi, 0, 0)$, M = $(\pi, \pi, 0)$, Z = $(0, 0, \pi)$, R = $(\pi, 0, \pi)$, and A = (π, π, π) points. According to LDA [34] the d_{z^2} band is almost fully filled and features a flat part that, however, lies near the Fermi energy only at $k_z = \pi$ momentum. In addition, the d_{z^2} band has an electron pocket around the Γ point that is hybridized with a slightly unoccupied SD band. The $d_{x^2-y^2}$ orbital appears to be metallic and nearly half-filled.

Local electronic correlations accounted for in the charge self-consistent combination [76] of DFT, self-interaction correction (SIC), and DMFT (DFT+sicDMFT framework [77]) change the occupation of bands to $\{1.83, 1.00, 0.17\}$ and consequently modify the electronic spectral function [34]. The latter is shown in Fig. 1 (see the inset for the color code). One

finds, that considering local correlations results in the shift of the flat part of the d_{z^2} band (high-intensity weight plotted in magenta) closer to the Fermi energy and also makes the $d_{x^2-y^2}$ orbital Mott insulating (low-intensity weight at large energies plotted in yellow). Nevertheless, the d_{z^2} (magenta) and SD (cyan) bands remain metallic, which makes the NdNiO₂ an orbital-selective Mott insulator [34].

To account for nonlocal correlation effects beyond DMFT, we perform D-TRILEX calculations for the model Hamiltonian (1) that describes the low-energy part of the electronic spectrum. In this model, only two of three orbitals are considered correlated, so introducing electronic interactions will shift the position of correlated d_{z^2} and $d_{x^2-y^2}$ bands with respect to the uncorrelated SD one. In order to reproduce the correct position of the bands, one has to compensate this shift by introducing the double-counting (DC) correction, i.e. the constant shift μ^{DC} , for the d_{z^2} and $d_{x^2-y^2}$ orbitals (see, e.g., Ref. [34]). In the DFT+sicDMFT framework the DC correction is usually determined from the self-consistent calculation of the Hartree-Fock-like shift, which is related to the occupation of orbitals. In D-TRILEX, a self-consistent determination of μ^{DC} would require solving the DMFT impurity problem for the single- and two-particle quantities and performing the D-TRILEX diagrammatic calculation at every iteration of a self-consistent cycle. This procedure is enormously time-consuming and is unfeasible in practice. We should also note that the value of the DC correction determined in this way is not exact, as it is related to the Hartree-Fock-like approximation. In this work we chose another root and perform a scan over a certain range of DC corrections following Ref. [78]. This procedure allows us to investigate sensitivity of correlation effects to μ^{DC} in the unique case when one of the correlated orbitals (d_{z^2}) features the flat band near the Fermi level. The resulting occupation of the bands obtained for different values of the DC correction is compared to the ones of the DFT+sicDMFT scheme to determine the most consistent μ^{DC} . To identify the range of values for μ^{DC} we calculate the Hartree-Fock shift induced by electronic interactions for the d_{z^2} and $d_{x^2-y^2}$ orbitals. This shift can be obtained from the form of the interaction part of the Hamiltonian (1) and reads:

$$\mu_{z^2}^{\text{DC}} = \frac{U}{2}n_{z^2} + \frac{2U' - J}{2}n_{x^2-y^2}, \quad (2)$$

$$\mu_{x^2-y^2}^{\text{DC}} = \frac{U}{2}n_{x^2-y^2} + \frac{2U' - J}{2}n_{z^2}. \quad (3)$$

Substituting the DFT+sicDMFT values for the occupations gives $\mu_{z^2}^{\text{DC}} = 10.9 \equiv \mu_z$ and $\mu_{x^2-y^2}^{\text{DC}} = 11.7 \equiv \mu_{xy}$, which sets the lower and upper bounds for μ^{DC} , respectively.

For the identified range of DC values we first perform calculations in the absence of the electron-phonon coupling for the fixed total occupation of $n_{\text{total}} = 3$ electrons per three bands. We begin by solving the DMFT impurity problem, which is done separately for each considered value of μ^{DC} . After that, the exact impurity Green’s function, susceptibilities and vertex functions are used to construct the D-TRILEX diagrammatic expansion [50–52]. Within this work all cal-

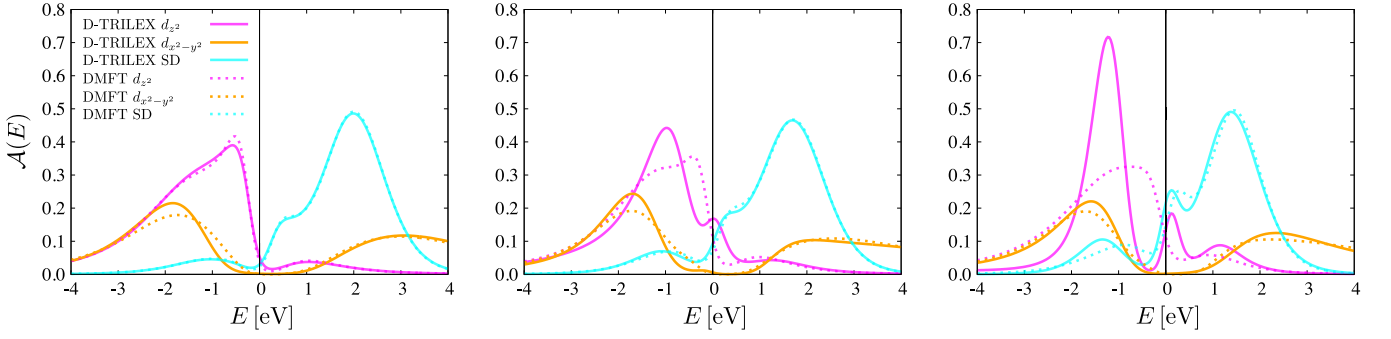


FIG. 2. Band-resolved local electronic spectral functions. Results are obtained for d_{z^2} (magenta), $d_{x^2-y^2}$ (orange), and SD (cyan) bands for μ_{xy} (left panel), $\mu^{\text{DC}} = 11.2$ (middle panel), and μ_z (right panel). The D-TRILEX and DMFT results are shown in solid and dashed lines, respectively. The system demonstrates the orbital-selective Mott behavior: The $d_{x^2-y^2}$ is half-filled and displays two Hubbard bands. The d_{z^2} and SD bands remain metallic for all considered μ^{DC} . Decreasing μ^{DC} results in a stronger attraction between the d_{z^2} and SD bands leading to the development of sharp peaks in each spectral function that merge in the vicinity of the Fermi energy at μ_z .

culations are done for a fixed temperature $T = 0.1$ eV. At this temperature the system lies in the paramagnetic phase close to the magnetic instability. In order to estimate the strength of the charge and spin fluctuations, we use the leading eigenvalue (LEV) of the Bethe-Salpeter equation (BSE) for the charge and spin susceptibility [52]. The spin LEV at the chosen temperature is $\text{LEV} \approx 0.75$ as shown in Table I. Therefore, in this temperature regime the spin fluctuations are already strong, as $\text{LEV} = 1$ would indicate the divergence of the susceptibility upon the transition to the ordered state. The corresponding eigenvector $\mathbf{q} = \text{M}$ shows that the leading instability in the spin channel corresponds to an in-plane (C-type) antiferromagnetic (AFM) ordering, which is consistent with experimental [79] observations and previous theoretical predictions [24, 30, 80, 81].

The occupation of bands obtained in D-TRILEX for different μ^{DC} are specified in Table I. These results suggest that μ_{xy} is the most consistent value of the DC correction, as it identically reproduces the occupation of bands found in DFT+sicDMFT [34]. In agreement with the DFT+sicDMFT calculations we find that taking into account correlation effects makes the $d_{x^2-y^2}$ band half filled for every considered value of μ^{DC} : $n_{x^2-y^2} = 1.00$ in D-TRILEX instead of

$n_{x^2-y^2} = 0.93$ in LDA. This fact explains why the change in μ^{DC} makes almost no influence on the strength (spin LEV, Table I) of spin fluctuations. We note, that for the largest considered value of the DC correction μ_{xy} the occupation of bands is redistributed by reducing n_{SD} , while the filling of the d_{z^2} band remains nearly unchanged compared to the LDA value. We also note, that for μ_{xy} the occupation of bands predicted by D-TRILEX coincides with one obtained within the DFT+sicDMFT scheme [34]. On the contrary, for $\mu^{\text{DC}} \approx 11.4$ the situation is reversed, and now the half filling of the $d_{x^2-y^2}$ band is achieved by reducing the occupation of the d_{z^2} band, while the occupation of the SD band is similar to the LDA one. Reducing the value of the DC correction to μ_z redistributes the occupation of bands in such a way, that the filling of the SD band becomes substantially larger than the one obtained in LDA and in DFT+sicDMFT.

In contrast to the nearly unchanged spin LEV, the charge LEV increases substantially with decreasing μ^{DC} . Thus, Table I shows that for the most consistent DC correction μ_{xy} the charge fluctuations are basically absent in the system ($\text{LEV} = 0.02$). Reducing μ^{DC} to μ_z drives the system in the region close to the CDW instability ($\text{LEV} = 0.95$) that is characterised by the ordering vector $\mathbf{q}_{\text{CDW}} = \text{X}$. We find, that the CDW ordering vector remains unchanged for all values of μ^{DC} at which the charge fluctuations are well developed ($\text{LEV} \geq 0.34$). Remarkably, we find that the formation of the CDW is unrelated to the usual mechanisms behind the charge instability, namely the electron-phonon coupling and long-range Coulomb interaction that were not taken into account in these calculations. As we show below, considering phonon degrees of freedom does not affect the formation of the CDW ordering. In turn, the realistic value of the nonlocal Coulomb interaction in NbNiO_2 is too small ($V \approx U/12$ [17]) to make any influence on the charge instability.

To identify the source of the CDW instability let us first look at the local electronic spectral function $\mathcal{A}(E)$ shown in Fig. 2 for the three different values of μ^{DC} . We find that for the most consistent μ_{xy} the spectral function of D-TRILEX (solid

TABLE I. The occupation of bands n_i , the LEV of the BSE for the charge and spin susceptibilities and the corresponding eigenvectors \mathbf{q} . Results are obtained for different values of μ^{DC} . All calculations, except for the last row, are performed in the absence of the electron-phonon (e-ph) coupling.

μ^{DC}	n_{z^2}	$n_{x^2-y^2}$	n_{SD}	charge LEV (\mathbf{q})	spin LEV (\mathbf{q})
11.7	1.83	1.00	0.17	0.02 (M)	0.72 (M)
11.5	1.80	1.00	0.20	0.16 (M)	0.75 (M)
11.4	1.78	1.00	0.22	0.34 (X)	0.75 (M)
11.2	1.73	1.00	0.27	0.64 (X)	0.77 (M)
11.0	1.70	1.00	0.30	0.83 (X)	0.76 (M)
10.9	1.65	1.00	0.35	0.95 (X)	0.74 (M)
10.9 (e-ph)	1.62	1.00	0.38	0.95 (X)	0.74 (M)

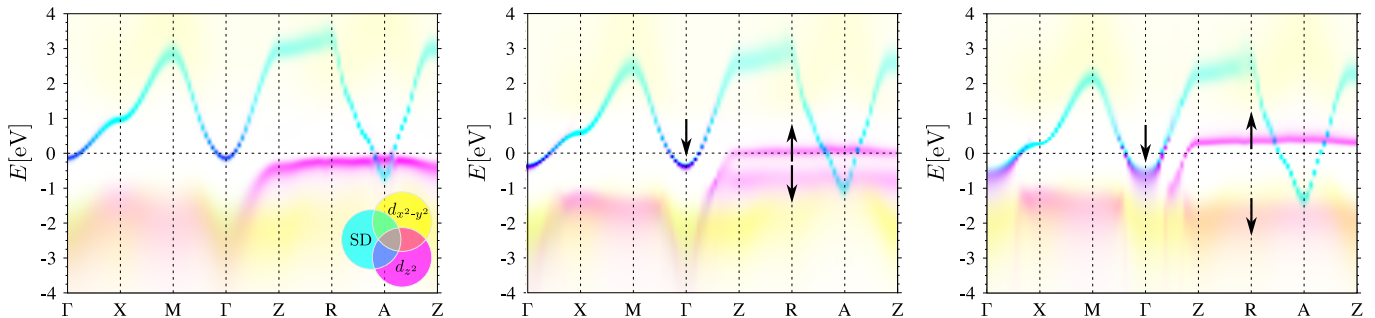


FIG. 3. Momentum-resolved electronic spectral functions. Results are obtained for the d_{z^2} , $d_{x^2-y^2}$, and SD bands (see the inset in the right panel for the color code) for μ_{xy} (left panel), $\mu^{\text{DC}} = 11.2$ (middle panel), and μ_z (right panel) along the high-symmetry path in the BZ. The low-intensity part of the spectrum at high energies plotted in yellow corresponds to Hubbard bands of the half-filled $d_{x^2-y^2}$ orbital. The high-intensity part of the spectrum around the Fermi energy plotted in magenta corresponds to the d_{z^2} orbital that displays a flat band feature at $k_z = \pi$. The black arrows depict the shift of the Γ point and of the flat part of the d_{z^2} band upon decreasing μ^{DC} .

lines) is very similar to the one of DMFT (dashed lines). Both methods predict a Mott insulating behavior for the half-filled $d_{x^2-y^2}$ band, while the d_{z^2} and SD bands remain metallic for all values of μ^{DC} . Therefore, the D-TRILEX approach also finds an orbital-selective Mott insulating behavior for NdNiO₂ in agreement with the previous DMFT calculation [34]. It is important to point out that this state is not destroyed by the magnetic fluctuations [63], because the metallic d_{z^2} and SD bands have a non-integer filling (see Table I), which suppresses the strength of the magnetic fluctuations. We observe, that decreasing μ^{DC} makes the DMFT result qualitatively unchanged, but the form of the local spectral function predicted by D-TRILEX changes substantially. First, we note that in D-TRILEX the Hubbard d_{z^2} bands, which for μ_{xy} appear at $E \approx -2$ eV and $E \approx 3$ eV, move closer to the Fermi energy E_F . Second, reducing the value of μ^{DC} increases the attraction between the d_{z^2} and SD bands. This fact is evident from the development of peaks in the corresponding (magenta and cyan) D-TRILEX spectral functions near the Fermi energy E_F (middle panel) that eventually merge at the same energy (right panel) when the system approaches the CDW transition point. This attraction seems to be realized through the spatial collective electronic fluctuations as it is not captured by DMFT.

To investigate the effect of spatial electronic correlations in more detail, let us look at the momentum-resolved spectral function shown in Fig. 3 for the d_{z^2} (magenta), $d_{x^2-y^2}$ (yellow), and SD (cyan) bands. The result is obtained using D-TRILEX for μ_{xy} (left panel), $\mu^{\text{DC}} = 11.2$ (middle panel), and μ_z (right panel). The dispersive low-intensity “yellow” weight at small and large energies corresponds to the Hubbard $d_{x^2-y^2}$ bands. The dispersive high-intensity “magenta” weight near the Fermi energy is the metallic d_{z^2} band that displays a flat feature at $k_z = \pi$. We point out, that for all considered values of μ^{DC} the d_{z^2} band reveals a momentum-dependent hybridization with the other bands. The hybridization of the d_{z^2} and SD bands around the Γ point results in the formation of the electron pocket. At $k_z = 0$ the d_{z^2} band hybridizes with the lower Hubbard $d_{x^2-y^2}$ band that lies at $E \approx -2$ eV.

We find that tuning μ^{DC} leads to a strong momentum-

dependent renormalization of the electronic spectral function, and, in particular, of the d_{z^2} band. This effect cannot be captured on the basis of local theories and requires an advanced combination of the band structure theory with the momentum-dependent many-body approach. The most striking change concerns the flat part of the d_{z^2} band. At the largest DC correction μ_{xy} this part lies below E_F (left panel in Fig. 3). Upon decreasing μ^{DC} the flat band splits into two parts that move in the opposite directions in energy as depicted by the black arrows in Fig. 3. One part moves toward the Fermi energy and at $\mu^{\text{DC}} = 11.2$ appears at E_F (middle panel). The other part moves toward lower energies and at μ_z hybridizes with the lower Hubbard $d_{x^2-y^2}$ band (right panel). Remarkably, at μ_z , when the system approaches the CDW transition point, the upper part of the flat band moves above the Fermi energy and becomes unoccupied. From this fact one can conclude that the CDW instability in NdNiO₂ is not related to the flat band feature. Remarkably, we find that in the vicinity of the CDW phase transition the position in energy of the flat part of the d_{z^2} band coincides with the position of the van Hove singularity (vHS) of the SD band located at the X point. This fact was ob-

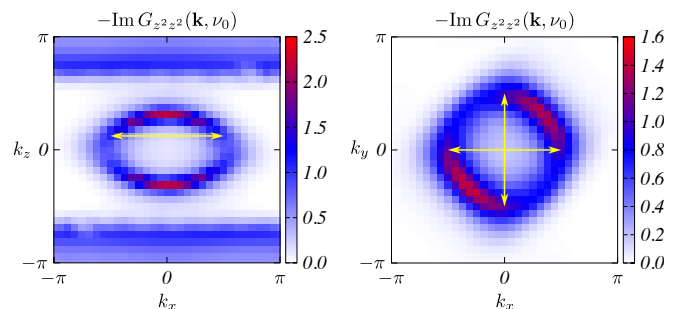


FIG. 4. The Fermi surface. The 2D cuts of the Fermi surface in the $(k_x, 0, k_z)$ (left panel) and $(k_x, k_y, \pi/8)$ (right panel) calculated near the CDW instability for μ_z . The FS is approximated by the imaginary part of the lattice Green’s function taken at the zeroth Matsubara frequency $-\text{Im} G_{z^2 z^2}(\mathbf{k}, \nu_0)$. The CDW ordering vectors \mathbf{q}_{CDW} connecting FS are shown in yellow arrows.

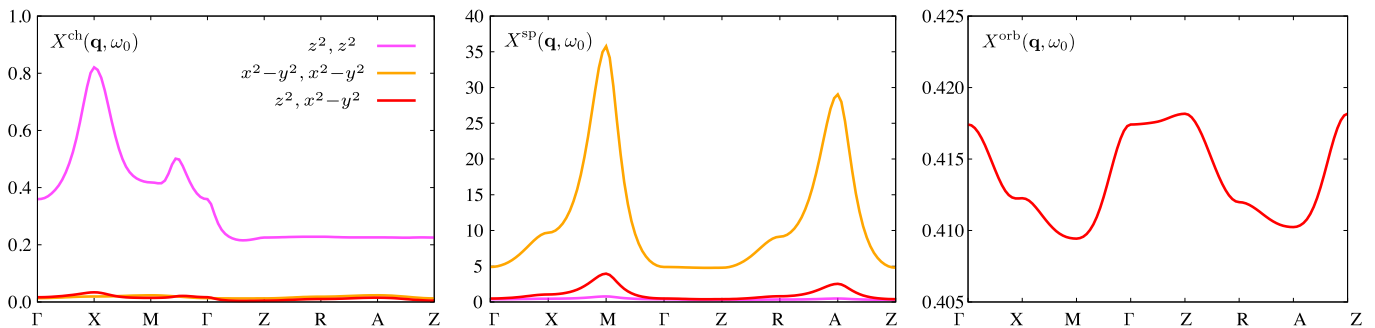


FIG. 5. Static susceptibilities. The absolute value of the band-resolved static charge (left panel), spin (middle panel) and orbital (right panel) susceptibility $X_{ll'}^{\text{ch/sp}}(\mathbf{q})$ calculated for $l, l' \in \{d_{z^2}, d_{x^2-y^2}\}$ bands along the high-symmetry path in the BZ. The leading contributions to the charge and spin susceptibilities originate respectively from the intraband collective electronic fluctuations in the d_{z^2} and $d_{x^2-y^2}$ bands. The orbital fluctuations between the d_{z^2} and $d_{x^2-y^2}$ bands are rather small and predominantly local. The result is obtained in the proximity to the CDW instability achieved for the DC correction μ_z .

served in the local spectral function as the attraction between the d_{z^2} and SD bands manifested itself with two (magenta and cyan) matching peaks near E_F (right panel in Fig. 2).

Another drastic change in the spectral function occurs in the vicinity of the Γ point, where the hybridized d_{z^2} and the SD bands form an electron pocket. We note that this pocket contains a relatively large spectral weight. Upon reducing μ^{DC} the Γ point moves to lower energies causing an enhancement of the electron pocket in order to compensate the shift of the upper part of the flat band in the opposite direction. These observations suggest that the CDW instability originates from the nesting of the Fermi surface (FS) related to the electron pocket of the d_{z^2} band, as the SD band is uncorrelated. Remarkably, at μ_z , when the system is in the vicinity of the CDW phase transition, the Γ point moves to such low energies that it leads to a hybridization of the d_{z^2} and SD bands with the lower Hubbard $d_{x^2-y^2}$ band at this k-point (right panel in Fig. 3).

We approximate the FS by the imaginary part of the lattice Green's function ($-\text{Im}G(\mathbf{k}, \nu_n)$) taken at the zeroth fermionic Matsubara frequency ν_0 . The CDW ordering vector $\mathbf{q}_{\text{CDW}} = \text{X}$ suggests that the two-particle scattering between the FS points occurs at a constant momenta k_z and k_x (or k_y). For this reason, in Fig. 4 we plot the 2D cuts of the FS in the $(k_x, 0, k_z)$ (left panel) and $(k_x, k_y, \pi/8)$ (right panel) obtained in the vicinity of the CDW ordering for μ_z . Plotting the \mathbf{q}_{CDW} vectors explicitly (yellow arrows) suggests that the electronic scattering that leads to the formation of the CDW ordering occurs for $k_z \simeq \pi/8$ and $k_x(k_y) = 0$.

The conclusion that the CDW instability originates from the electronic scattering within the d_{z^2} band is also confirmed by the form of the charge susceptibility. Fig. 5 shows the absolute value of the static (ω_0) D-TRILEX charge (left panel), spin (bottom panel) and orbital (right panel) susceptibility [52] $X_{ll'}^{\text{ch/sp}}(\mathbf{q}, \omega_n)$ obtained for the correlated $l, l' \in \{d_{z^2}, d_{x^2-y^2}\}$ bands along the high-symmetry path in the BZ. We find, that the dominant contribution to the charge susceptibility originates from the intraband d_{z^2} component that reveals a peak at exactly the \mathbf{q}_{CDW} wave vector. The charge

susceptibility also displays a subleading mode corresponding to the wave vector $\mathbf{q} \simeq (0.3\pi, 0.3\pi, 0)$. We note, that the previous DMFT calculation performed for the distorted crystal structure corresponding to the CDW phases obtained in DFT calculations predicted the $\mathbf{q} = (\pi/3, \pi/3, 0)$ wave vector for the CDW modulation [82]. On the contrary, the leading contribution to the spin susceptibility comes from the intraband $d_{x^2-y^2}$ component. The highest peak in the spin susceptibility at the $\mathbf{q} = \text{M}$ point indicates that the leading magnetic instability corresponds to the in-plane AFM (C-AFM) ordering. This fact is also evident from the eigenvector $\mathbf{q} = \text{M}$ corresponding to the LEV of the spin fluctuations (Table I), as has been discussed above. However, a relatively high peak at the $\mathbf{q} = \text{A}$ point indicates that the G-type AFM fluctuations in the system are also rather strong. The competition between the C- and G-types of AFM ordering has also been predicted for doped NdNiO₂ in Ref. [83] based on the DMFT calculations. However, the G-type of AFM ordering was found to be dominant at stoichiometry. Finally, by looking at the right panel of Fig. 5, one finds that the orbital fluctuations between the d_{z^2} and $d_{x^2-y^2}$ bands are negligibly small and mainly local (constant in momentum space).

In order to illustrate the influence of the phonon degrees of freedom on the formation of the CDW ordering we repeat the same calculations in the presence of the electron-phonon coupling. We find that, besides a small difference in the occupation of the d_{z^2} and SD bands (bottom row of Table I), considering phonons does not affect the obtained results. Indeed, the strength and the ordering vectors of the charge and spin fluctuations remain the same as in the absence of the electron-phonon coupling (bottom row of Table I), and the electronic spectral function is barely changed (Fig. 6). The only noticeable difference is the fact that the half filling in these two cases is realized for different values of the chemical potential. To be precise, taking into account the electron phonon coupling results in the increase of the chemical potential by $\delta\mu \simeq 0.066$ eV. We note, however, that the Holstein model for phonon degrees of freedom may lead to an under-

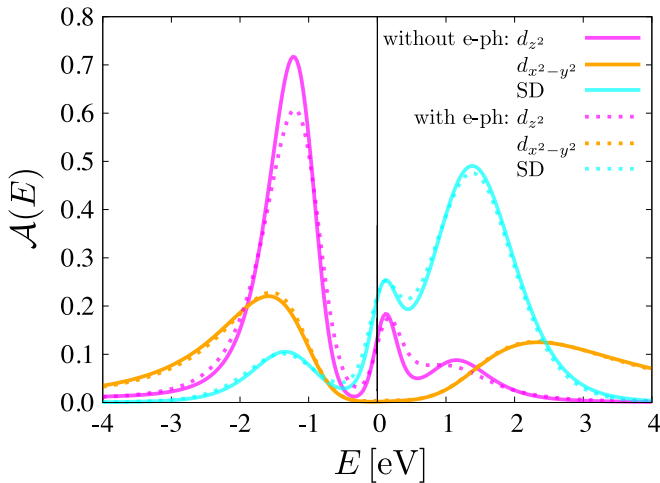


FIG. 6. The band-resolved local electronic spectral function. Results are obtained for d_{z^2} (magenta), $d_{x^2-y^2}$ (orange), and SD (cyan) bands without (solid lines) and with (dashed line) taking into account the electron-phonon (e-ph) coupling for μ_z .

estimate of the phonon contribution to the CDW instability, since in this case the phonon-mediated electronic interaction $U_{ll'}^{\text{ph}}(\omega)$ competes with the large intraorbital U and interorbital U' Coulomb interactions. Considering other types of the electron-phonon coupling, e.g. a Jahn-Teller or a momentum-dependent ones, may lead to a more noticeable effect [84].

In both cases (with and without accounting for the electron-phonon coupling) the large leading eigenvalue of the charge fluctuations $\text{LEV} = 0.95$ is found for the same DC correction μ_z (Table I). However, at this value of μ^{DC} the occupation of the SD band is already approximately two times larger and the occupation of the d_{z^2} band is substantially lower than the ones obtained within the DFT+sicDMFT framework [34]. In addition, the local spectral function calculated for μ_{xy} (left panel in Fig. 3) much better reproduces the experimentally observed photoemission spectrum [85, 86] than the one obtained for μ_z (right panel in Fig. 3). Indeed, a dominant first peak at $E \simeq -2$ eV seen in the experiments agrees well with the position of the lower Hubbard $d_{x^2-y^2}$ band obtained for μ_{xy} . For smaller μ^{DC} the Hubbard bands are shifted closer to the Fermi level. Furthermore, the experiments also do not observe sharp peaks due to a flat part of the d_{z^2} band appearing in the vicinity of E_F at stoichiometry. Note, that in DFT+sicDMFT such shift of the flat band only takes place for a sizable doping [34]. Therefore, the choice of μ_z does not correspond to the pristine NdNiO₂. On the other hand, in the case of μ_{xy} , which reproduces the DFT+sicDMFT occupation of bands, the charge fluctuations are absent in the system, as discussed above. Therefore, one can conclude that the CDW ordering cannot be found in NdNiO₂ at stoichiometry, which is in line with the results of recent experiments [12, 13, 16].

CDW upon hole doping. According to the results obtained at half filling the CDW instability in NdNiO₂ originates from the intraband scattering of electrons within the

TABLE II. The occupation of bands n_i , the LEV of the BSE for the charge and spin susceptibilities and the corresponding eigenvectors \mathbf{q} . Results are obtained for μ_{xy} in the presence of the electron-phonon coupling for different levels of the hole doping.

n_{total}	n_{z^2}	$n_{x^2-y^2}$	n_{SD}	charge LEV (\mathbf{q})	spin LEV (\mathbf{q})
2.96	1.78	1.00	0.18	0.49 (X)	0.74 (M)
2.92	1.75	1.00	0.17	0.63 (X)	0.77 (M)
2.89	1.72	1.00	0.17	0.74 (X)	0.76 (M)
2.83	1.66	1.00	0.17	0.89 (X)	0.76 (M)

d_{z^2} electron pocket and arises upon reducing the occupation of this band. The latter might be, in principle, achieved in a more physical way, i.e. upon hole doping the system. In order to understand if this results in the formation of the CDW ordering, we stick to the most consistent DC correction μ_{xy} and perform the D-TRILEX calculations for different levels of the hole doping. Similarly to the half-filled case considered above, we find that considering the electron-phonon coupling does not affect the physical behavior of the system. For this reason, in this section, we present only the results calculated in the presence of the electron-phonon coupling.

Table II shows the occupation of the bands, the LEV and the corresponding eigenvectors of the charge and spin fluctuations. We find that upon the hole doping the total density n_{total} is reduced by diminishing the occupation of the d_{z^2} band, while the occupation of the other two bands remains unchanged. In particular, the $d_{x^2-y^2}$ stays half-filled and Mott-insulating for all considered levels of the doping, which consequently leads to a nearly unchanged strength (spin LEV) of the leading C-type ($\mathbf{q} = \text{M}$) AFM fluctuations that stem from this band. This fact explains the intrinsic magnetic ground state that was detected experimentally for various superconducting infinite-layer nickelates irrespective of the rare earth ion or doping [87].

We find that the mechanism of the formation of the CDW ordering also remains the same as in the half-filled case. The only difference is that the reduction of n_{z^2} is achieved here by the hole doping instead of tuning μ^{DC} . As can be found from Table II, reducing the occupation of the d_{z^2} band consequently enhances the strength of the charge fluctuations, since they originate from the intraband electronic scattering within the d_{z^2} band. We observe that the momentum-dependent renormalization of the spectral function upon doping is qualitatively the same as upon changing μ^{DC} . In Fig. 7 the momentum-resolved spectral function is shown in the vicinity of the CDW instability (charge $\text{LEV} = 0.89$) induced by the doping ($n_{\text{total}} = 2.85$). We again notice the splitting of the flat part of the d_{z^2} band at $k_z = \pi$ into the two parts and the hybridization of its lower part with the lower Hubbard $d_{x^2-y^2}$ band. We also see that near the CDW instability the upper part of the flat band appears above the Fermi energy and thus does not participate in the two-particle scattering that results in the CDW instability. In turn, the Γ point of the d_{z^2} band is shifted to lower energies below E_F and forms the electron pocket.

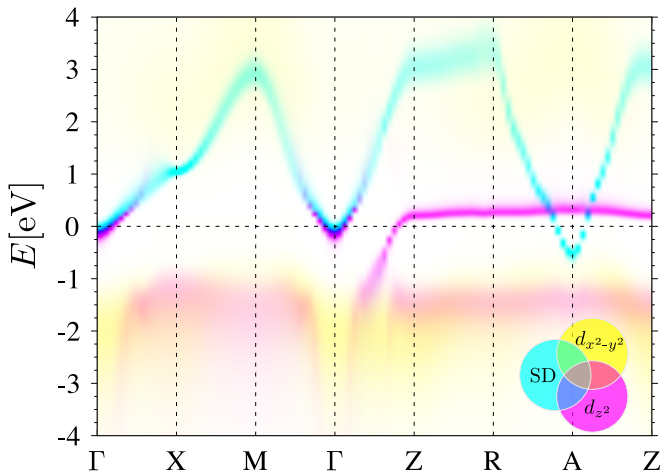


FIG. 7. The momentum-resolved electronic spectral function. The result is obtained for the d_{z^2} , $d_{x^2-y^2}$, and SD bands (see the inset for the color code) for μ_{xy} and $n_{\text{total}} = 2.83$ near the CDW instability (charge LEV = 0.89) along the high-symmetry path in the BZ.

Interestingly, the renormalization of the spectral function upon hole doping found in D-TRILEX is different from the one obtained within the DFT+sicDMFT scheme [34]. The latter predicts a rather uniform shift of the bands toward higher energies. In particular, DFT+sicDMFT the flat part of the d_{z^2} band does not split and moves from below to above the Fermi energy. The Γ point also shifts to positive energies, which removes the electron pocket from the Fermi level. Pinning the electron pocket to the Fermi energy upon doping observed in D-TRILEX is, therefore, an important effect of nonlocal electronic correlations, since this pocket plays a crucial role in the formation of the CDW ordering. In particular, this pinning explains why the CDW ordering vector $\mathbf{q}_{\text{CDW}} = \mathbf{X}$ remains unchanged for different doping levels (Table II). We note that the spectral function in Fig. 7 is plotted at a smaller charge LEV than the one in the right panel of Fig. 3 due to convergence issues while approaching the CDW instability in the doped case. For this reason, the flat part of the d_{z^2} band is not yet aligned with the vHS of the SD band, and the electron pocket at the Γ point is smaller than the one in the right panel of Fig. 3.

The critical density for the CDW transition can be obtained by looking at the evolution of the charge LEV as a function of doping. In Fig. 8 we plot the difference of the LEV from unity ($1 - \text{LEV}$) as a function of the total electronic density n_{total} . By extrapolating the $1 - \text{LEV}$ value to zero we get the $n_{\text{total}} \approx 2.79$ value for the critical density for the CDW phase transition. It is important to point out that the CDW instability that originates due to the Coulomb interaction (not via the electron-phonon mechanism) typically does not exhibit a strong dependence on temperature [47, 53, 88]. This allows us to speculate that the dip in the superconducting dome observed in the hole doped NdNiO_2 at the density $n_{\text{total}} \approx 2.80$ [1, 2] may arise due to a competition of the superconductivity with strong CDW fluctuations. A similar conclusion was made in the recent experimental work [43], where

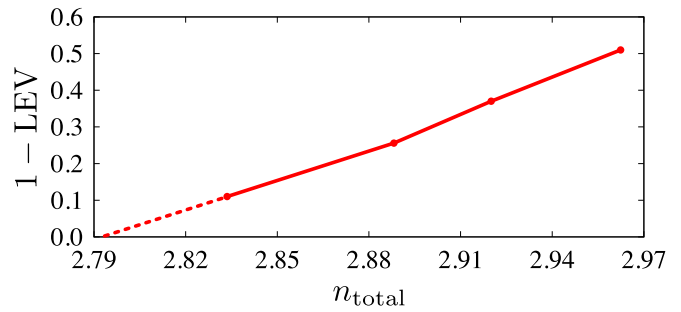


FIG. 8. The evolution of the charge LEV as a function of the hole doping. To estimate the critical value of the doping we plot the ($1 - \text{LEV}$) value that becomes zero at the transition point. The results are obtained in the presence of the coupling. According to a linear fit performed for the two lowest points the critical density for the CDW phase transition in the presence of phonons is $n_{\text{total}} \approx 2.79$.

the rotational symmetry breaking observed in superconducting $\text{Nd}_{0.8}\text{Sr}_{0.2}\text{NiO}_2$ films was associated with the charge order. We also wish to point out, that the doping level at which these measurements were performed is similar to the critical density for the CDW phase transition obtained in the current work.

In Fig. 9 we plot the spectral functions (susceptibilities) for collective charge (left column), spin (middle column) and orbital (right column) fluctuations as a function of real energy E along the high-symmetry path in the BZ. The result is obtained for the most consistent DC correction μ_{xy} at half-filling (top row) and in the vicinity of the CDW instability for $n_{\text{total}} \approx 2.83$ (bottom row). These results visualise the evolution of the collective electronic fluctuations with doping discussed above. At stoichiometry the charge fluctuations are negligibly small (top left panel) and dominated by the low energy (static) contribution. The spin fluctuations are also static and display the leading $\mathbf{q} = \mathbf{M}$ (C-type) and the subleading $\mathbf{q} = \mathbf{A}$ (G-type) AFM modes that have a comparable intensity (top middle panel). We note that dispersive spin excitations (magnons) are not visible in this plot because the calculations are performed close to the magnetic instability, and thus almost all spectral weight is moved to the ordering AFM modes. Instead, the orbital fluctuations are dynamic with the characteristic energy of $E \approx 1.5 - 2.0$ eV but are rather small and nearly momentum-independent (top right panel).

Upon approaching the CDW instability the charge spectral function reduces to a two-peak structure with the main mode at $\mathbf{q} = \mathbf{X}$, which will lead to the CDW ordering upon the transition, and a small satellite peak at $\mathbf{q} = (\pi/3, \pi/3, 0)$ (bottom left panel). In turn, the spin spectral function still reveals two AFM modes (bottom middle panel). However, the subleading mode in the doped case is more suppressed with respect to the leading compared to the half-filled case. The competition between the C- and G-type AFM ordering that at large doping levels reduces to the C-type one has also been found in the previous DMFT calculation [83]. Finally, orbitals fluctuations remain qualitatively unchanged upon doping, but become slightly weaker and broader in energy.

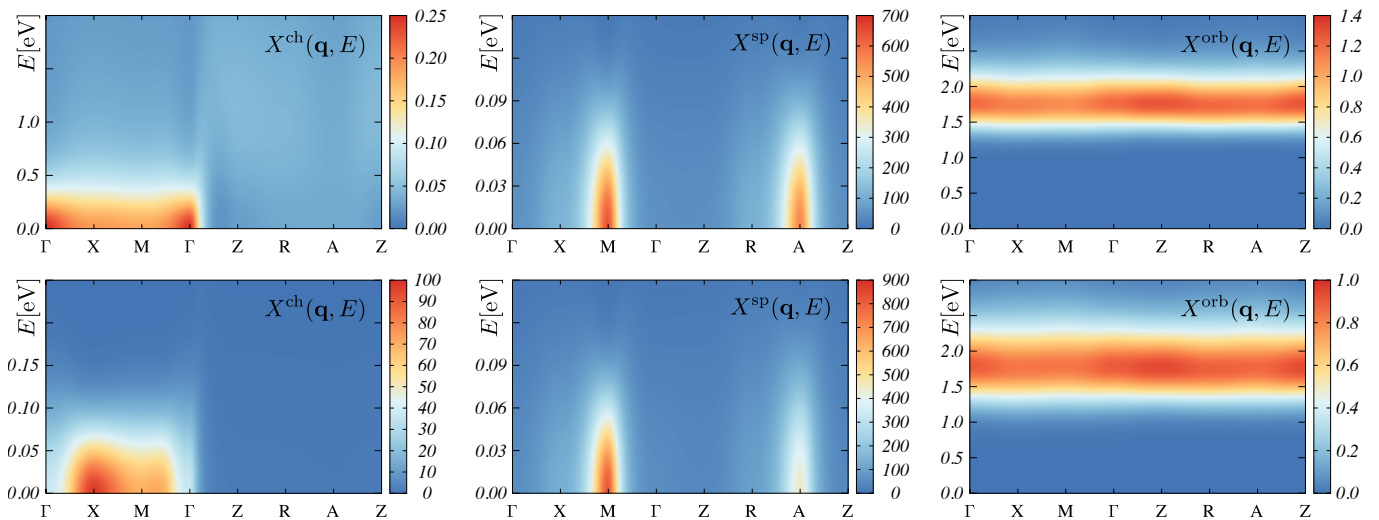


FIG. 9. Momentum-resolved spectral functions for collective electronic fluctuations. Charge (left panels), spin (middle panels) and orbital (right panels) spectral functions (susceptibilities) calculated as a function of real energy E . Results are obtained for μ_{xy} for the correlated d_{z^2} and $d_{x^2-y^2}$ bands along the high-symmetry path in the BZ. Calculation are performed at half filling (top row) and at $n_{\text{total}} = 2.83$ (bottom row).

DISCUSSION

In this work we investigated the effect of collective electronic fluctuations in the infinite-layer NdNiO₂ at stoichiometry and upon hole doping. We have shown that the electronic correlations that lead to the CDW and magnetic instabilities in this system are orbital-dependent. We have found that the strong CDW fluctuations are related to electronic correlations within the d_{z^2} orbital. Upon doping, these fluctuations drive the material toward the CDW ordered phase when considering only possible particle-hole instabilities. The mechanism of this transition relies on the strong momentum-dependent renormalization of the electronic spectral function. This renormalization consists of splitting and moving one part of the flat region of the d_{z^2} band from below to above the Fermi energy, where it aligns in energy with the vHS of the SD band. The other part of the flat band is moved in the opposite direction, where it hybridizes with the lower Hubbard $d_{x^2-y^2}$ band. In turn, the Γ point of the hybridized d_{z^2} and SD bands is shifted toward smaller energies, which enlarges the electron pocket around the vicinity of the Γ point. As a result, the flat part of the band does not take part in the formation of the CDW phase, that instead occurs due to the nesting of the Fermi surface in the $(k_x, k_y, \pi/8)$ plane.

We argue that this complex momentum-dependent renormalization of the electronic spectral function, which is associated with a rather large redistribution of the electronic density between the orbitals, is unlikely to happen in the stoichiometric case. This means that the formation of the CDW ordering cannot be found in the pristine NdNiO₂, which is also confirmed by the most recent experiments [12, 13, 16]. Instead, we demonstrate that the same renormalization can be obtained upon hole doping leading to the CDW phase transition at a critical density $n_{\text{total}} \approx 2.79$. Remarkably, we find that

the nonlocal electronic correlations pin the electron pocket of the Ni- d_{z^2} band, which is responsible for the formation of the CDW ordering, to the Fermi energy even upon hole doping. This observation challenges the single-band picture of the electronic correlations in nickelates, which partially originates from the DMFT prediction that the electron pocket becomes unimportant upon doping as it shifts well above the Fermi level (see, e.g., Ref. [34]).

We also find that the strong magnetic fluctuations originate from the intraband electronic correlations within a completely different, namely the $d_{x^2-y^2}$, orbital. Our calculations show that the electronic correlations redistribute the density between the orbitals in such a way that the $d_{x^2-y^2}$ band remains half-filled. Remarkably, the filling of the $d_{x^2-y^2}$ band remains unchanged upon hole doping, which, consequently, results in a nearly unchanged strength of magnetic fluctuations that consist of the leading C- and the subleading G-type AFM modes. These results show that both, CDW and magnetic fluctuations are strong in the hole doped regime of NdNiO₂ and can thus affect superconductivity in this compound.

METHODS

The three-orbital Hubbard-Holstein-Kanamori Hamiltonian (1) that models the NdNiO₂ compound is solved using the many-body diagrammatic D-TRILEX approach [50–52]. This method is a dual version [89–97] of the TRILEX approach [98–101], where the nonlocal electronic correlations are taken into account by means of the diagrammatic expansion constructed on the basis of an interacting reference problem. The latter is chosen in such a way that it can be solved numerically exactly, e.g., by using the continuous time quantum Monte Carlo (CT-QMC) solvers [56–59]. This

sets certain limitations on the form of the reference system. In particular, in the multi-band case the advanced CT-QMC solvers are usually restricted to a static interaction. For this reason, in this work we perform D-TRILEX calculations based on the DMFT reference impurity problem that involves only the static interaction $U_{l_1 l_2 l_3 l_4}$. The frequency-dependent interaction $U_{ll' ll'}^{\text{ph}}(\omega)$ that originates from the electron-phonon coupling is treated diagrammatically in the same way as one would account for the nonlocal Coulomb interaction [50–52]. The impurity problem is solved using the w2DYNAMICS package [60]. All calculations are performed for $N_k = 32^3$ number of \mathbf{k} -points in the BZ. The local and momentum-resolved electronic, charge, spin and orbital spectral functions are obtained from the corresponding Matsubara Green's functions and susceptibilities via analytical continuation using the maximum entropy method implemented in the ANA_CONT package [102]. The charge and spin susceptibilities are obtained using D-TRILEX, as described in Ref. 52.

Data Availability. The data that support the findings of this work are available from the corresponding author upon reasonable request.

Code Availability. Many-body calculations have been performed using the implementation of the D-TRILEX method [52]. The D-TRILEX code is available from the corresponding author upon reasonable request.

Funding. A.I.L. acknowledges the support by the DFG through FOR 5249-449872909 (Project P8) and by the European Research Council via Synergy Grant 854843-FASTCORR. E.A.S. acknowledges the help of the CPHT computer support team.

Author contributions. All authors discussed the results and contributed to the preparation of the manuscript.

Competing Interests. The Authors declare no Competing Financial or Non-Financial Interests.

-
- [1] Danfeng Li, Bai Yang Wang, Kyuho Lee, Shannon P. Harvey, Motoki Osada, Berit H. Goodge, Lena F. Kourkoutis, and Harold Y. Hwang, “Superconducting Dome in $\text{Nd}_{1-x}\text{Sr}_x\text{NiO}_2$ Infinite Layer Films,” *Phys. Rev. Lett.* **125**, 027001 (2020).
- [2] Shengwei Zeng, Chi Sin Tang, Xinmao Yin, Changjian Li, Mengsha Li, Zhen Huang, Junxiong Hu, Wei Liu, Ganesh Ji Omar, Hariom Jani, Zhi Shiuh Lim, Kun Han, Dongyang Wan, Ping Yang, Stephen John Pennycook, Andrew T. S. Wee, and Ariando Ariando, “Phase Diagram and Superconducting Dome of Infinite-Layer $\text{Nd}_{1-x}\text{Sr}_x\text{NiO}_2$ Thin Films,” *Phys. Rev. Lett.* **125**, 147003 (2020).
- [3] Motoki Osada, Bai Yang Wang, Berit H. Goodge, Kyuho Lee, Hyeok Yoon, Keita Sakuma, Danfeng Li, Masashi Miura, Lena F. Kourkoutis, and Harold Y. Hwang, “A Superconducting Praseodymium Nickelate with Infinite Layer Structure,” *Nano Lett.* **20**, 5735 (2020).
- [4] Motoki Osada, Bai Yang Wang, Berit H. Goodge, Shannon P. Harvey, Kyuho Lee, Danfeng Li, Lena F. Kourkoutis, and Harold Y. Hwang, “Nickelate Superconductivity without Rare-Earth Magnetism: $(\text{La,Sr})\text{NiO}_2$,” *Adv. Mater.* **33**, 2104083 (2021).
- [5] Shengwei Zeng, Changjian Li, Lin Er Chow, Yu Cao, Zhaoting Zhang, Chi Sin Tang, Xinmao Yin, Zhi Shiuh Lim, Junxiong Hu, Ping Yang, and Ariando Ariando, “Superconductivity in infinite-layer nickelate $\text{La}_{1-x}\text{Ca}_x\text{NiO}_2$ thin films,” *Sci. Adv.* **8**, eab19927 (2022).
- [6] Grace A. Pan, Dan Ferenc Segedin, Harrison LaBollita, Qi Song, Emilian M. Nica, Berit H. Goodge, Andrew T. Pierce, Spencer Doyle, Steve Novakov, Denisse Córdova Carrizales, Alpha T. N’Diaye, Padraic Shafer, Hanjong Paik, John T. Heron, Jarad A. Mason, Amir Yacoby, Lena F. Kourkoutis, Onur Erten, Charles M. Brooks, Antia S. Botana, and Julia A. Mundy, “Superconductivity in a quintuple-layer square-planar nickelate,” *Nat. Mater.* **21**, 160–164 (2021).
- [7] Hualei Sun, Mengwu Huo, Xunwu Hu, Jingyuan Li, Yifeng Han, Lingyun Tang, Zhongqian Mao, Pengtao Yang, Bosen Wang, Jinguang Cheng, Dao-Xin Yao, Guang-Ming Zhang, and Meng Wang, “Signatures of superconductivity near 80 K in a nickelate under high pressure,” *Nature* **621**, 493–498 (2023).
- [8] Matteo Rossi, Motoki Osada, Jaewon Choi, Stefano Agrestini, Daniel Jost, Yonghun Lee, Haiyu Lu, Bai Yang Wang, Kyuho Lee, Abhishek Nag, Yi-De Chuang, Cheng-Tai Kuo, Sang-Jun Lee, Brian Moritz, Thomas P. Devereaux, Zhi-Xun Shen, Jun-Sik Lee, Ke-Jin Zhou, Harold Y. Hwang, and Wei-Sheng Lee, “A broken translational symmetry state in an infinite-layer nickelate,” *Nat. Phys.* **18**, 869–873 (2022).
- [9] G. Krieger, L. Martinelli, S. Zeng, L. E. Chow, K. Kummer, R. Arpaia, M. Moretti Sala, N. B. Brookes, A. Ariando, N. Viart, M. Salluzzo, G. Ghiringhelli, and D. Preziosi, “Charge and Spin Order Dichotomy in NdNiO_2 Driven by the Capping Layer,” *Phys. Rev. Lett.* **129**, 027002 (2022).
- [10] Charles C. Tam, Jaewon Choi, Xiang Ding, Stefano Agrestini, Abhishek Nag, Mei Wu, Bing Huang, Huiqian Luo, Peng Gao, Mirian García-Fernández, Liang Qiao, and Ke-Jin Zhou, “Charge density waves in infinite-layer NdNiO_2 nickelates,” *Nat. Mater.* **21**, 1116–1120 (2022).
- [11] Xiaolin Ren, Ronny Sutarto, Qiang Gao, Qisi Wang, Jiarui Li, Yao Wang, Tao Xiang, Jiangping Hu, Fu-Chun Zhang, J. Chang, Riccardo Comin, X. J. Zhou, and Zhihai Zhu, “Symmetry of Charge Order in Infinite-layer Nickelates,” Preprint arXiv:2303.02865 (2023).
- [12] Raji, Aravind and Krieger, Guillaume and Viart, Nathalie and Preziosi, Daniele and Rueff, Jean-Pascal and Gloter, Alexandre, “Charge distribution across capped and uncapped infinite-layer neodymium nickelate thin films,” *Small*, 2304872 (2023).
- [13] C. T. Parzyck, N. K. Gupta, Y. Wu, V. Anil, L. Bhatt, M. Bouliane, R. Gong, B. Z. Gregory, A. Luo, R. Sutarto, F. He, Y. D. Chuang, T. Zhou, G. Herranz, L. F. Kourkoutis, A. Singer, D. G. Schlom, D. G. Hawthorn, and K. M. Shen, “Absence of $3a_0$ Charge Density Wave Order in the Infinite Layer Nickelates,” Preprint arXiv:2307.06486 (2023).
- [14] J. Pellicciari, N. Khan, P. Wasik, A. Barbour, Y. Li, Y. Nie, J. M. Tranquada, V. Bisogni, and C. Mazzoli, “Comment on newly found Charge Density Waves in infinite layer Nickelates,” Preprint arXiv:2306.15086 (2023).
- [15] Charles C. Tam, Jaewon Choi, Xiang Ding, Stefano Agrestini, Abhishek Nag, Mei Wu, Bing Huang, Huiqian Luo, Peng Gao, Mirian Garcia-Fernandez, Liang Qiao, and Ke-Jin Zhou, “Reply to ‘Comment on newly found Charge Density Waves in infinite layer Nickelates,’” Preprint arXiv:2307.13569 (2023).

- [16] S. Hayashida, V. Sundaramurthy, P. Puphal, M. Garcia-Fernandez, Ke-Jin Zhou, B. Fenk, M. Isobe, M. Minola, Y. M. Wu, Y. E. Suyolcu, P. A. van Aken, B. Keimer, and M. Heping, “Investigation of spin excitations and charge order in bulk crystals of the infinite-layer nickelate LaNiO_2 ,” Preprint arXiv:2403.00493 (2024).
- [17] Yusuke Nomura, Motoaki Hirayama, Terumasa Tadano, Yoshihide Yoshimoto, Kazuma Nakamura, and Ryotaro Arita, “Formation of a two-dimensional single-component correlated electron system and band engineering in the nickelate superconductor NdNiO_2 ,” *Phys. Rev. B* **100**, 205138 (2019).
- [18] Frank Lechermann, “Late transition metal oxides with infinite-layer structure: Nickelates versus cuprates,” *Phys. Rev. B* **101**, 081110 (2020).
- [19] V. Yu. Irkhin, A. A. Katanin, and M. I. Katsnelson, “Effects of van Hove singularities on magnetism and superconductivity in the $t-t'$ Hubbard model: A parquet approach,” *Phys. Rev. B* **64**, 165107 (2001).
- [20] A. P. Kampf and A. A. Katanin, “Competing phases in the extended $U-V-J$ Hubbard model near the Van Hove fillings,” *Phys. Rev. B* **67**, 125104 (2003).
- [21] Walter Metzner, Manfred Salmhofer, Carsten Honerkamp, Volker Meden, and Kurt Schönhammer, “Functional renormalization group approach to correlated fermion systems,” *Rev. Mod. Phys.* **84**, 299–352 (2012).
- [22] Xianxin Wu, Domenico Di Sante, Tilman Schwemmer, Werner Hanke, Harold Y. Hwang, Srinivas Raghu, and Ronny Thomale, “Robust $d_{x^2-y^2}$ -wave superconductivity of infinite-layer nickelates,” *Phys. Rev. B* **101**, 060504 (2020).
- [23] Guang-Ming Zhang, Yi-feng Yang, and Fu-Chun Zhang, “Self-doped Mott insulator for parent compounds of nickelate superconductors,” *Phys. Rev. B* **101**, 020501 (2020).
- [24] Jonathan Karp, Antia S. Botana, Michael R. Norman, Hyowon Park, Manuel Zingl, and Andrew Millis, “Many-Body Electronic Structure of NdNiO_2 and CaCuO_2 ,” *Phys. Rev. X* **10**, 021061 (2020).
- [25] I. Leonov, S. L. Skornyakov, and S. Y. Savrasov, “Lifshitz transition and frustration of magnetic moments in infinite-layer NdNiO_2 upon hole doping,” *Phys. Rev. B* **101**, 241108 (2020).
- [26] Priyo Adhikary, Subhadeep Bandyopadhyay, Tanmoy Das, Indra Dasgupta, and Tanusri Saha-Dasgupta, “Orbital-selective superconductivity in a two-band model of infinite-layer nickelates,” *Phys. Rev. B* **102**, 100501 (2020).
- [27] Motoharu Kitatani, Liang Si, Oleg Janson, Ryotaro Arita, Zhicheng Zhong, and Karsten Held, “Nickelate superconductors - a renaissance of the one-band Hubbard model,” *npj Quantum Mater.* **5**, 59 (2020).
- [28] Emily Been, Wei-Sheng Lee, Harold Y. Hwang, Yi Cui, Jan Zaanen, Thomas Devereaux, Brian Moritz, and Chunjing Jia, “Electronic Structure Trends Across the Rare-Earth Series in Superconducting Infinite-Layer Nickelates,” *Phys. Rev. X* **11**, 011050 (2021).
- [29] Benjamin Geisler and Rossitza Pentcheva, “Correlated interface electron gas in infinite-layer nickelate versus cuprate films on $\text{SrTiO}_3(001)$,” *Phys. Rev. Res.* **3**, 013261 (2021).
- [30] Yuhao Gu, Sichen Zhu, Xiaoxuan Wang, Jiangping Hu, and Hanghui Chen, “A substantial hybridization between correlated Ni-d orbital and itinerant electrons in infinite-layer nickelates,” *Commun. Physics* **3**, 84 (2020).
- [31] Tharathep Plienbumrung, Maria Daghofer, Michael Schmid, and Andrzej M. Oleś, “Screening in a two-band model for superconducting infinite-layer nickelate,” *Phys. Rev. B* **106**, 134504 (2022).
- [32] Mi Jiang, Mona Berciu, and George A. Sawatzky, “Critical Nature of the Ni Spin State in Doped NdNiO_2 ,” *Phys. Rev. Lett.* **124**, 207004 (2020).
- [33] Philipp Werner and Shintaro Hoshino, “Nickelate superconductors: Multiorbital nature and spin freezing,” *Phys. Rev. B* **101**, 041104(R) (2020).
- [34] Frank Lechermann, “Multiorbital Processes Rule the $\text{Nd}_{1-x}\text{Sr}_x\text{NiO}_2$ Normal State,” *Phys. Rev. X* **10**, 041002 (2020).
- [35] Francesco Petocchi, Viktor Christiansson, Fredrik Nilsson, Ferdi Aryasetiawan, and Philipp Werner, “Normal State of $\text{Nd}_{1-x}\text{Sr}_x\text{NiO}_2$ from Self-Consistent $GW + \text{EDMFT}$,” *Phys. Rev. X* **10**, 041047 (2020).
- [36] Chang-Jong Kang and Gabriel Kotliar, “Optical Properties of the Infinite-Layer $\text{La}_{1-x}\text{Sr}_x\text{NiO}_2$ and Hidden Hund’s Physics,” *Phys. Rev. Lett.* **126**, 127401 (2021).
- [37] Andreas Kreisel, Brian M. Andersen, Astrid T. Rømer, Ilya M. Eremin, and Frank Lechermann, “Superconducting Instabilities in Strongly Correlated Infinite-Layer Nickelates,” *Phys. Rev. Lett.* **129**, 077002 (2022).
- [38] Sebastien N. Abadi, Ke-Jun Xu, Eder G. Lomeli, Pascal Puphal, Masahiko Isobe, Yong Zhong, Alexei V. Fedorov, Sung-Kwan Mo, Makoto Hashimoto, Dong-Hui Lu, Brian Moritz, Bernhard Keimer, Thomas P. Devereaux, Matthias Heping, and Zhi-Xun Shen, “Electronic structure of the alternating monolayer-trilayer phase of $\text{La}_3\text{Ni}_2\text{O}_7$,” Preprint arXiv:2402.07143 (2024).
- [39] Antoine Georges, Gabriel Kotliar, Werner Krauth, and Marcelo J. Rozenberg, “Dynamical mean-field theory of strongly correlated fermion systems and the limit of infinite dimensions,” *Rev. Mod. Phys.* **68**, 13–125 (1996).
- [40] Paul Worm, Qisi Wang, Motoharu Kitatani, Izabela Biało, Qiang Gao, Xiaolin Ren, Jaewon Choi, Diana Csontosová, Ke-Jin Zhou, Xingjiang Zhou, Zhihai Zhu, Liang Si, Johan Chang, Jan M. Tomczak, and Karsten Held, “Spin fluctuations sufficient to mediate superconductivity in nickelates,” Preprint arXiv:2312.08260 (2023).
- [41] Yang Shen, Mingpu Qin, and Guang-Ming Zhang, “Comparative study of charge order in undoped infinite-layer nickelate superconductors,” *Phys. Rev. B* **107**, 165103 (2023).
- [42] Hanghui Chen, Yi feng Yang and Guang Ming Zhang, and Hongquan Liu, “Comparative study of charge order in undoped infinite-layer nickelate superconductors,” *Nat. Commun.* **14**, 5477 (2023).
- [43] Haoran Ji, Yanan Li, Yi Liu, Xiang Ding, Zheyuan Xie, Shichao Qi, Liang Qiao, Yi feng Yang, Guang-Ming Zhang, and Jian Wang, “Rotational symmetry breaking in superconducting nickelate $\text{Nd}_{0.8}\text{Sr}_{0.2}\text{NiO}_2$ films,” *Nat. Commun.* **14**, 7155 (2023).
- [44] E. Berger, P. Valášek, and W. von der Linden, “Two-dimensional Hubbard-Holstein model,” *Phys. Rev. B* **52**, 4806–4814 (1995).
- [45] G. Sangiovanni, M. Capone, C. Castellani, and M. Grilli, “Electron-Phonon Interaction Close to a Mott Transition,” *Phys. Rev. Lett.* **94**, 026401 (2005).
- [46] Philipp Werner and Andrew J. Millis, “Efficient Dynamical Mean Field Simulation of the Holstein-Hubbard Model,” *Phys. Rev. Lett.* **99**, 146404 (2007).
- [47] E. A. Stepanov, V. Harkov, M. Rösner, A. I. Lichtenstein, M. I. Katsnelson, and A. N. Rudenko, “Coexisting charge density wave and ferromagnetic instabilities in monolayer InSe ,” *npj Comput. Mater.* **8**, 118 (2022).
- [48] G. Rohringer, H. Hafermann, A. Toschi, A. A. Katanin, A. E. Antipov, M. I. Katsnelson, A. I. Lichtenstein, A. N. Rubtsov,

- and K. Held, “Diagrammatic routes to nonlocal correlations beyond dynamical mean field theory,” *Rev. Mod. Phys.* **90**, 025003 (2018).
- [49] Ya. S. Lyakhova, G. V. Astretsov, and A. N. Rubtsov, “The mean-field concept and post-DMFT methods in the contemporary theory of correlated systems,” *PHYS-USP* **193**, 825–844 (2023), [Phys. Usp. 66 775–793 (2023)].
- [50] E. A. Stepanov, V. Harkov, and A. I. Lichtenstein, “Consistent partial bosonization of the extended Hubbard model,” *Phys. Rev. B* **100**, 205115 (2019).
- [51] V. Harkov, M. Vandelli, S. Brener, A. I. Lichtenstein, and E. A. Stepanov, “Impact of partially bosonized collective fluctuations on electronic degrees of freedom,” *Phys. Rev. B* **103**, 245123 (2021).
- [52] Matteo Vandelli, Josef Kaufmann, Mohammed El-Nabulsi, Viktor Harkov, Alexander I. Lichtenstein, and Evgeny A. Stepanov, “Multi-band D-TRILEX approach to materials with strong electronic correlations,” *SciPost Phys.* **13**, 036 (2022).
- [53] M. Vandelli, A. Galler, A. Rubio, A. I. Lichtenstein, S. Biermann, and E. A. Stepanov, “Doping-dependent charge- and spin-density wave orderings in a monolayer of Pb adatoms on Si(111),” *npj Quantum Mater.* **9**, 19 (2024).
- [54] Maria Chatzieftheriou, Silke Biermann, and Evgeny A. Stepanov, “Local and nonlocal electronic correlations at the metal-insulator transition in the Hubbard model in two dimensions,” Preprint arXiv:2312.03123 (2023).
- [55] Evgeny A. Stepanov, Maria Chatzieftheriou, Niklas Wagner, and Giorgio Sangiovanni, “Interconnected Renormalization of Hubbard Bands and Green’s Function Zeros in Mott Insulators Induced by Strong Magnetic Fluctuations,” Preprint arXiv:2402.02814 (2024).
- [56] A. N. Rubtsov, V. V. Savkin, and A. I. Lichtenstein, “Continuous-time quantum Monte Carlo method for fermions,” *Phys. Rev. B* **72**, 035122 (2005).
- [57] Philipp Werner, Armin Comanac, Luca de’ Medici, Matthias Troyer, and Andrew J. Millis, “Continuous-time solver for quantum impurity models,” *Phys. Rev. Lett.* **97**, 076405 (2006).
- [58] Philipp Werner and Andrew J. Millis, “Dynamical screening in correlated electron materials,” *Phys. Rev. Lett.* **104**, 146401 (2010).
- [59] Emanuel Gull, Andrew J. Millis, Alexander I. Lichtenstein, Alexey N. Rubtsov, Matthias Troyer, and Philipp Werner, “Continuous-time Monte Carlo methods for quantum impurity models,” *Rev. Mod. Phys.* **83**, 349–404 (2011).
- [60] Markus Wallerberger, Andreas Hausoel, Patrik Gunacker, Alexander Kowalski, Nicolaus Parragh, Florian Goth, Karsten Held, and Giorgio Sangiovanni, “w2dynamics: Local one- and two-particle quantities from dynamical mean field theory,” *Computer Physics Communications* **235**, 388–399 (2019).
- [61] Evgeny A. Stepanov, Yusuke Nomura, Alexander I. Lichtenstein, and Silke Biermann, “Orbital Isotropy of Magnetic Fluctuations in Correlated Electron Materials Induced by Hund’s Exchange Coupling,” *Phys. Rev. Lett.* **127**, 207205 (2021).
- [62] M. Vandelli, J. Kaufmann, V. Harkov, A. I. Lichtenstein, K. Held, and E. A. Stepanov, “Extended regime of metastable metallic and insulating phases in a two-orbital electronic system,” *Phys. Rev. Res.* **5**, L022016 (2023).
- [63] Evgeny A. Stepanov, “Eliminating Orbital Selectivity from the Metal-Insulator Transition by Strong Magnetic Fluctuations,” *Phys. Rev. Lett.* **129**, 096404 (2022).
- [64] Evgeny A. Stepanov and Silke Biermann, “Can Orbital-Selective Néel Transitions Survive Strong Nonlocal Electronic Correlations?” Preprint arXiv:2305.16730 (2023).
- [65] Hiroshi Shinaoka, Dominique Geffroy, Markus Wallerberger, Junya Otsuki, Kazuyoshi Yoshimi, Emanuel Gull, and Jan Kuneš, “Sparse sampling and tensor network representation of two-particle Green’s functions,” *SciPost Phys.* **8**, 012 (2020).
- [66] Anna Galler, Patrik Thunström, Patrik Gunacker, Jan M. Tomczak, and Karsten Held, “Ab initio dynamical vertex approximation,” *Phys. Rev. B* **95**, 115107 (2017).
- [67] Anna Galler, Josef Kaufmann, Patrik Gunacker, Matthias Pickem, Patrik Thunström, Jan M. Tomczak, and Karsten Held, “Towards ab initio Calculations with the Dynamical Vertex Approximation,” *J. Phys. Soc. Jpn.* **87**, 041004 (2018).
- [68] Josef Kaufmann, Christian Eckhardt, Matthias Pickem, Motoharu Kitatani, Anna Kauch, and Karsten Held, “Self-consistent ladder dynamical vertex approximation,” *Phys. Rev. B* **103**, 035120 (2021).
- [69] M. Vandelli, *Quantum embedding methods in dual space for strongly interacting electronic systems*, Ph.D. thesis, Universität Hamburg, Hamburg (2022).
- [70] Lars Hedin, “New Method for Calculating the One-Particle Green’s Function with Application to the Electron-Gas Problem,” *Phys. Rev.* **139**, A796–A823 (1965).
- [71] E. A. Stepanov, S. Brener, F. Krien, M. Harland, A. I. Lichtenstein, and M. I. Katsnelson, “Effective Heisenberg Model and Exchange Interaction for Strongly Correlated Systems,” *Phys. Rev. Lett.* **121**, 037204 (2018).
- [72] D. Geffroy, J. Kaufmann, A. Hariki, P. Gunacker, A. Hausoel, and J. Kuneš, “Collective Modes in Excitonic Magnets: Dynamical Mean-Field Study,” *Phys. Rev. Lett.* **122**, 127601 (2019).
- [73] Lorenzo Del Re and Alessandro Toschi, “Dynamical vertex approximation for many-electron systems with spontaneously broken SU(2) symmetry,” *Phys. Rev. B* **104**, 085120 (2021).
- [74] I. A. Goremykin and A. A. Katanin, “Commensurate and spiral magnetic order in the doped two-dimensional Hubbard model: Dynamical mean-field theory analysis,” *Phys. Rev. B* **107**, 245104 (2023).
- [75] Lorenzo Del Re, “Two-particle self-consistent approach for broken symmetry phases,” Preprint arXiv:2312.16280 (2024).
- [76] Daniel Grieger, Christoph Piefke, Oleg E. Peil, and Frank Lechermann, “Approaching finite-temperature phase diagrams of strongly correlated materials: A case study for V₂O₃,” *Phys. Rev. B* **86**, 155121 (2012).
- [77] Frank Lechermann, Wolfgang Körner, Daniel F. Urban, and Christian Elsässer, “Interplay of charge-transfer and Mott-Hubbard physics approached by an efficient combination of self-interaction correction and dynamical mean-field theory,” *Phys. Rev. B* **100**, 115125 (2019).
- [78] M. Karolak, G. Ulm, T. Wehling, V. Mazurenko, A. Poteryaev, and A. Lichtenstein, “Double counting in LDA+DMFT—The example of NiO,” *J. Electron Spectros. Relat. Phenomena* **181**, 11–15 (2010), proceedings of International Workshop on Strong Correlations and Angle-Resolved Photoemission Spectroscopy 2009.
- [79] Yi Cui, Cong Li, Qing Li, Xiyu Zhu, Ze Hu, Yifeng Yang, Jinshan Zhang, Rong Yu, Hai-Hu Wen, and Weiqiang Yu, “NMR Evidence of Antiferromagnetic Spin Fluctuations in Nd_{0.85}Sr_{0.15}NiO₂,” *Chinese Physics Letters* **38**, 067401 (2021).
- [80] Frank Lechermann, “Doping-dependent character and possible magnetic ordering of NdNiO₂,” *Phys. Rev. Mater.* **5**, 044803 (2021).
- [81] Jonathan Karp, Alexander Hampel, and Andrew J. Millis, “Superconductivity and antiferromagnetism in NdNiO₂ and CaCuO₂: A cluster DMFT study,” *Phys. Rev. B* **105**, 205131

- (2022).
- [82] K. G. Slobodchikov and I. V. Leonov, “Spin density wave, charge density wave, and bond disproportionation wave instabilities in hole-doped infinite-layer $RNiO_2$,” *Phys. Rev. B* **106**, 165110 (2022).
- [83] I. Leonov, “Effect of lattice strain on the electronic structure and magnetic correlations in infinite-layer $(Nd,Sr)NiO_2$,” *J. Alloys Compd.* **883**, 160888 (2021).
- [84] Alberto Scazzola, Adriano Amaricci, and Massimo Capone, “Competing correlated insulators in multiorbital systems coupled to phonons,” *Phys. Rev. B* **107**, 085131 (2023).
- [85] Berit H. Goodge, Danfeng Li, Kyuho Lee, Motoki Osada, Bai Yang Wang, George A. Sawatzky, Harold Y. Hwang, and Lena F. Kourkoutis, “Doping evolution of the mott–hubbard landscape in infinite-layer nickelates,” *Proceedings of the National Academy of Sciences* **118**, e2007683118 (2021).
- [86] Zhuoyu Chen, Motoki Osada, Danfeng Li, Emily M. Been, Su-Di Chen, Makoto Hashimoto, Donghui Lu, Sung-Kwan Mo, Kyuho Lee, Bai Yang Wang, Fanny Rodolakis, Jessica L. McChesney, Chunjing Jia, Brian Moritz, Thomas P. Devereaux, Harold Y. Hwang, and Zhi-Xun Shen, “Electronic structure of superconducting nickelates probed by resonant photoemission spectroscopy,” *Matter* **5**, 1806–1815 (2022).
- [87] Jennifer Fowlie, Marios Hadjimichael, Maria M Martins, Danfeng Li, Motoki Osada, Bai Yang Wang, Kyuho Lee, Yonghun Lee, Zaher Salman, Thomas Prokscha, Jean-Marc Triscone, Harold Y. Hwang, and Andreas Suter, “Intrinsic magnetism in superconducting infinite-layer nickelates,” *Nat. Phys.* **18**, 1043–1047 (2022).
- [88] Hanna Terletska, Tianran Chen, and Emanuel Gull, “Charge ordering and correlation effects in the extended hubbard model,” *Phys. Rev. B* **95**, 115149 (2017).
- [89] A. N. Rubtsov, M. I. Katsnelson, and A. I. Lichtenstein, “Dual fermion approach to nonlocal correlations in the Hubbard model,” *Phys. Rev. B* **77**, 033101 (2008).
- [90] A. N. Rubtsov, M. I. Katsnelson, A. I. Lichtenstein, and A. Georges, “Dual fermion approach to the two-dimensional Hubbard model: Antiferromagnetic fluctuations and Fermi arcs,” *Phys. Rev. B* **79**, 045133 (2009).
- [91] H. Hafermann, G. Li, A. N. Rubtsov, M. I. Katsnelson, A. I. Lichtenstein, and H. Monien, “Efficient perturbation theory for quantum lattice models,” *Phys. Rev. Lett.* **102**, 206401 (2009).
- [92] A. N. Rubtsov, M. I. Katsnelson, and A. I. Lichtenstein, “Dual boson approach to collective excitations in correlated fermionic systems,” *Ann. Phys.* **327**, 1320–1335 (2012).
- [93] Erik G. C. P. van Loon, Alexander I. Lichtenstein, Mikhail I. Katsnelson, Olivier Parcollet, and Hartmut Hafermann, “Beyond extended dynamical mean-field theory: Dual boson approach to the two-dimensional extended Hubbard model,” *Phys. Rev. B* **90**, 235135 (2014).
- [94] E. A. Stepanov, E. G. C. P. van Loon, A. A. Katanin, A. I. Lichtenstein, M. I. Katsnelson, and A. N. Rubtsov, “Self-consistent dual boson approach to single-particle and collective excitations in correlated systems,” *Phys. Rev. B* **93**, 045107 (2016).
- [95] E. A. Stepanov, A. Huber, E. G. C. P. van Loon, A. I. Lichtenstein, and M. I. Katsnelson, “From local to nonlocal correlations: The Dual Boson perspective,” *Phys. Rev. B* **94**, 205110 (2016).
- [96] L. Peters, E. G. C. P. van Loon, A. N. Rubtsov, A. I. Lichtenstein, M. I. Katsnelson, and E. A. Stepanov, “Dual boson approach with instantaneous interaction,” *Phys. Rev. B* **100**, 165128 (2019).
- [97] M. Vandelli, V. Harkov, E. A. Stepanov, J. Gukelberger, E. Kozik, A. Rubio, and A. I. Lichtenstein, “Dual boson diagrammatic Monte Carlo approach applied to the extended Hubbard model,” *Phys. Rev. B* **102**, 195109 (2020).
- [98] Thomas Ayrat and Olivier Parcollet, “Mott physics and spin fluctuations: A unified framework,” *Phys. Rev. B* **92**, 115109 (2015).
- [99] Thomas Ayrat and Olivier Parcollet, “Mott physics and spin fluctuations: A functional viewpoint,” *Phys. Rev. B* **93**, 235124 (2016).
- [100] J. Vučičević, T. Ayrat, and O. Parcollet, “TRILEX and $GW+EDMFT$ approach to d -wave superconductivity in the Hubbard model,” *Phys. Rev. B* **96**, 104504 (2017).
- [101] Thomas Ayrat, Jaksu Vučičević, and Olivier Parcollet, “Fierz convergence criterion: A controlled approach to strongly interacting systems with small embedded clusters,” *Phys. Rev. Lett.* **119**, 166401 (2017).
- [102] Josef Kaufmann and Karsten Held, “ana_cont: Python package for analytic continuation,” Preprint arXiv:2105.11211 (2021).